Nonlinear Asymptotic Impedance Model for a Helmholtz Resonator of Finite Depth

Sjoerd W. Rienstra* and Deepesh Kumar Singh†
Dept. of Mathematics and Computer Science, TU Eindhoven, The Netherlands

A systematic derivation of the solution of a nonlinear system of equations for the finite-length Helmholtz resonator is presented, modelling the configuration of an organ-pipe type cavity (*i.e.* of finite length) connected via an acoustically small neck to the external excitation field. The model of the flow through the neck includes linear viscous friction and nonlinear dissipation due to vortex shedding. By assuming a weakly nonlinear amplitude regime, *i.e.* essentially nonlinear near resonance but effectively linear away from resonance, we are able to set up a solution, asymptotic for small excitation amplitudes, which enables us to obtain analytically an expression for the impedance that includes nonlinear effects for frequencies close to the fundamental resonance frequency. (The higher harmonics will not be considered).

This paper extends and refines our previous analysis that considered an acoustically compact cavity. Apart from a confirmation of the previously published impedance results in the small cavity limit, the new results establish a significant improvement in the comparison with experimental data and the asymptotic matching of the linear and nonlinear impedance regimes. This is for a part due to the obviously refined model of the geometry, but also due to the equivalent but numerically better alternative form of the asymptotic expressions that, by chance, emerged in the new analysis. Although both versions are asymptotically equivalent to the order considered, the new form happens to behave better for larger values of the excitation amplitude.

Keywords: Non-linear Impedance, Acoustic Liner, Weakly Non-linear Oscillations, Perturbation Methods

I. Introduction

The sound emission from aircraft engines, power machines and several other industrial applications is a matter of high concern that affects the community noise and hence health and life. In most of the applications, the emission spectrum is concentrated near a few prominent frequencies that are in general attenuated with the help of liners. An important type of acoustic liner for aero-engine inlet and exhaust ducts constitutes of a honeycomb array of small cells called Helmholtz resonators. The Helmholtz resonator is a cavity filled with air and having a small opening called the neck (Fig. 1). When excited with a fluctuating external pressure, the mass of the air plug inside the neck moves against the large volume of compressible air inside the cavity, which acts as a spring, while viscous forces and vortex shedding cause dissipation of energy.

*Associate Professor, Dept. Math. & Comp. Sc., T.U. Eindhoven, Netherlands, Senior Member AIAA.
†Doctoral candidate, Dept. Mathematics & Computer Science, T.U. Eindhoven, Netherlands.

In its simplest form, for wavelengths much larger than the size of the cavity, this establishes a weakly nonlinear 0−D mass-spring-damper system. The damping is normally relatively small such that a resonance frequency can be identified. At and near resonance, the dissipation is largest and so narrow band sound absorption is achieved for frequencies close to resonance. Properties of this process form the basic design criterion for the liners. The resonator, as "seen" from outside, is characterized by its impedance $Z = Z(\omega)$, relating (spatially averaged) pressure and velocity at the wall. Ideally, Z is a wall property, independent of the acoustic field. However, in particular near resonance, Z is amplitude dependent for high but relevant amplitudes, for example of the "buzz saw" noise in a turbofan engine due to the shocks produced in front of the fan at take-off and the blade tips operating near sonic conditions [1, 2]. It is important to know quantitatively and understand qualitatively such impedances Z with good precision to improve the design of the structures and have the highest possible attenuation of the emitted soundfield.

The nonlinear effects are mainly of hydrodynamical origin, due to the resistive losses and vortex shedding at inflow and outflow from the opening, as shown in Fig. 2. This is physically a process of great complexity [3, 4] which has indeed exacerbated the possibility to obtain the impedance with an accurate model based on first principles.

The nonlinear corrections of the impedance, common in the literature, are based on physically inspired modelling assumptions, but otherwise do not aim to solve the equations of the nonlinear resonator [5–7]. In contrast, the properties of the Helmholtz resonator have been obtained from the full equations in [1, 8–13], but these are all fully CFD, DNS or LES simulations which do not give information for the simpler models. The Helmholtz resonator equation which describes the neck region flow coupled with the cavity (Fig. 1) can be solved asymptotically with a closure condition that relates pressure and velocity inside the cavity near the neck. This was done in our previous paper [14]. The found impedance was favourably compared with the existing experimental data. The considered cavity was acoustically compact, *i.e.* the size of the cavity was much smaller than the acoustic wavelength $L \ll \lambda$, so that the pressure inside was nearly uniform and the neck velocity was simply given by the time derivative of the pressure. Hence the resonator acts like a spring to the external force.

In the present paper we improve this modelling assumption of a 0−D *vanishing* cavity size (compared to the acoustic wave length), by considering a 1−D cavity of *finite length*. We solve the wave equation inside the cavity to obtain a relationship between pressure and velocity of the waves developing inside the cavity. In this way, we capture more physics of the problem and the fidelity of the model is improved.

We follow much of the derivation done in [14], and focus on a systematic derivation of an asymptotic solution of a stand-alone nonlinear Helmholtz resonator equation from first principles. The extra complication of grazing flow along the liner wall will not be considered here. This effect is important if the mean flow boundary layer is thin enough and the resonator outflow velocity is comparable to (or higher than) the mean flow velocity.

We start with the classical modelling of the Helmholtz resonator and formulate a perturbation problem in terms of a small parameter ε which is based on the excitation amplitude of a given pressure of fixed frequency. The stationary solution of this problem is solved asymptotically. Secular effects of the external forcing are treated in the usual way by a suitable Lindstedt-Poincaré type approach. A non-standard problem is the modulus term $|u|$ of the velocity. This prohibits a standard asymptotic expansion because the location of the zeros of u are a priori unknown. This problem has been tackled by adding an unknown shift of the origin, to be determined along with the construction of the solution, and using the fact that the stationary solution has the same periodicity as the driving force.

II. Mathematical formulation

The organ-pipe type resonator, *i.e.* the resonator of finite length considered here, is shown in Fig 1. The base area of the cavity of length L is S_b and the cross sectional area of the neck is S_n. It should be noted that this neck area is to be interpreted as the *effective* cross section. In other words, the geometric cross section multiplied by a discharge coefficient, to include what is commonly known as the *vena contracta* effect (due to separation of the streamlines at the opening edge). This will normally be a weak function of the amplitude, but is assumed to be constant here. Unless we know this discharge coefficient by other means, S_n is a modelling parameter.

The frequency of the external excitation is assumed to be low enough that crosswise higher order modes are cut off in the cavity region of length L, leading to only plane waves inside. Considering that the cavity neck ℓ is acoustically compact *i.e.* $k\ell \ll 1$ for a typical wavenumber $k = \omega/c_0$, we can neglect compressibility in the neck and determine the line integral of the momentum equation (with mean density ρ_0, velocity $\boldsymbol{v}$ and pressure perturbation p)

$$\rho_0\Big(\frac{\partial \boldsymbol{v}}{\partial t} + \boldsymbol{v}\cdot\nabla\boldsymbol{v}\Big) + \nabla p = \mu\nabla^2\boldsymbol{v}$$

along a streamline from a point inside to a point outside to obtain the relation

$$\rho_0 \int_{\text{in}}^{\text{ex}} \frac{\partial \boldsymbol{v}}{\partial t}\cdot\mathbf{d}\boldsymbol{s} + \tfrac{1}{2}\rho_0(v_{\text{ex}}^2 - v_{\text{in}}^2) + (p_{\text{ex}} - p_{\text{in}}) = \int_{\text{in}}^{\text{ex}} \mu\nabla^2\boldsymbol{v}\cdot\mathbf{d}\boldsymbol{s}, \tag{1}$$

with $v = \|\boldsymbol{v}\|$ and μ denoting the viscosity. Following Melling [5] we average pressure and velocity along the neck's cross section, assume that the averaged squared velocity is approximately equal to the squared averaged velocity, and obtain

$$\rho_0 \int_{\text{in}}^{\text{ex}} \frac{\partial \overline{\boldsymbol{v}}}{\partial t}\cdot\mathbf{d}\boldsymbol{s} + \tfrac{1}{2}\rho_0(\overline{v}_{\text{ex}}^2 - \overline{v}_{\text{in}}^2) + (p_{\text{ex}} - p_{\text{in}}) = \int_{\text{in}}^{\text{ex}} \mu\overline{\nabla^2\boldsymbol{v}}\cdot\mathbf{d}\boldsymbol{s}. \tag{2}$$

Assuming that the streamline does not change in time, we have

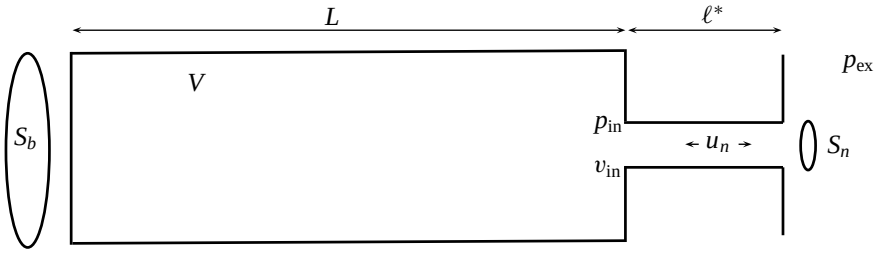

Figure 1. Resonator cavity and neck

$$\int_{\text{in}}^{\text{ex}} \frac{\partial \overline{\boldsymbol{v}}}{\partial t}\cdot\mathbf{d}\boldsymbol{s} = \frac{\mathrm{d}}{\mathrm{d}t}\int_{\text{in}}^{\text{ex}} \overline{\boldsymbol{v}}\cdot\mathbf{d}\boldsymbol{s}. \tag{3}$$

The velocity line integral evidently scales on a typical length times a typical velocity. If end effects are minor, we can use the neck flux velocity $\overline{\boldsymbol{v}} = u_n\boldsymbol{e}_x$ with a corresponding length being the neck length $\ell = \ell^* + \delta_1 + \delta_2$, consisting of the geometric neck length ℓ^* added by small end corrections δ_1 and δ_2 to take into account the inertia of the acoustic flow at both ends just outside the neck (inside and outside the resonator). Then we have

$$\int_{\text{in}}^{\text{ex}} \overline{\boldsymbol{v}}\cdot\mathbf{d}\boldsymbol{s} = \ell u_n. \tag{4}$$

For now, the geometry dependent end corrections δ are modelling parameters. They are assumed constant and known. For a number of geometries and ignoring viscosity, end corrections are given by Ingard [15]. For a circular orifice, for example, we may use $\delta = 0.85(S_n/\pi)^{1/2}$.

For the stress term line integral we observe that, apart from u_n itself, it will depend on flow profile, Reynolds number, wall heat exchange, turbulence, separation from sharp edges, and maybe more. Following Melling [5], we will take these effects together in a resistance factor R, which will be assumed relatively small, in order to have resonance and a small decay per period to begin with. We thus have

$$\int_{\text{in}}^{\text{ex}} \mu \overline{\nabla^2 \boldsymbol{v}} \cdot \mathbf{d}\boldsymbol{s} = -R u_n \tag{5}$$

(Note that this form is exact for a Poiseuille flow with parabolic profile). Unless we know this resistance factor by other means, R is a modelling parameter with (as will be detailed below) only a restriction on its order of magnitude to single out the relevant physical behaviour and to enable a consistent asymptotic analysis.

Due to separation from the outer exit, we have with outflow $\overline{v}_{\text{in}} \simeq 0$ with $\overline{v}_{\text{ex}} = u_n$ jetting out, while similarly during inflow, $\overline{v}_{\text{ex}} \simeq 0$ with $\overline{v}_{\text{in}} = u_n$ jetting into the cavity; see Fig. 2. The pressure in the jets, however, has to remain equal to the surrounding pressure (p_{ex} and p_{in} respectively) because the boundary of the jet cannot support a pressure difference. Therefore, we have altogether

$$\rho_0 \ell \frac{\mathrm{d}}{\mathrm{d}t} u_n + \tfrac{1}{2}\rho_0 u_n |u_n| + R u_n = p_{\text{in}} - p_{\text{ex}}. \tag{6}$$

The second equation between p_{in} and u_n is obtained by solving the wave equation in the

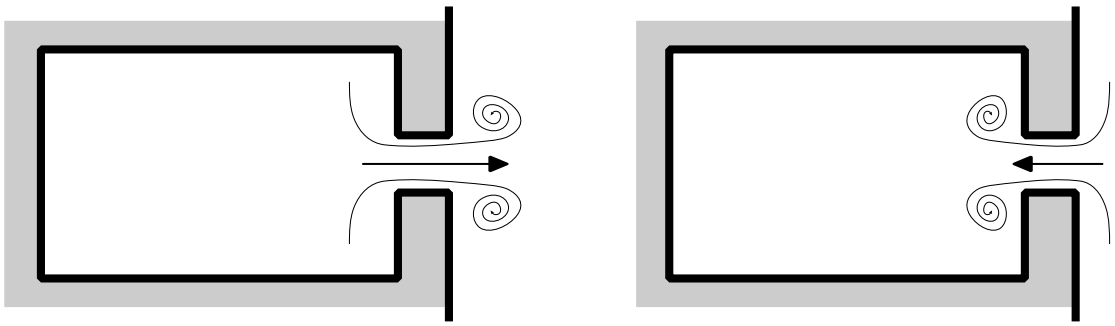

out-flow phase in-flow phase

Figure 2. Separation and vortex shedding during the out-flow and in-flow phase

attached cavity (pipe) of uniform cross section S_b and length L, located along $-L \leqslant x \leqslant 0$ where $x = 0$ is the position where the cavity connects to the neck. Inside the cavity, with axial velocity u and pressure perturbation p, we have

$$\begin{aligned} \frac{\partial p}{\partial t} + \rho_0 c_0^2 \frac{\partial u}{\partial x} &= 0 \\ \rho_0 \frac{\partial u}{\partial t} + \frac{\partial p}{\partial x} &= 0, \end{aligned} \tag{7}$$

with mean sound speed c_0 and assuming an adiabatic compression of the fluid in the cavity $p = c_0^2 \rho$ with density perturbation ρ. The end conditions are then

$$\begin{aligned} u(-L, t) &= 0 \\ p(0, t) &= p_{\text{in}}(t) \\ S_b u(0, t) &= S_n u_n(t). \end{aligned} \tag{8}$$

Using d'Alembert's solution we can solve (7) to obtain

$$\begin{aligned} p(x,t) &= \rho_0 c_0^2 (f(c_0 t - x - L) + f(c_0 t + x + L)) \\ u(x,t) &= \quad c_0 (f(c_0 t - x - L) - f(c_0 t + x + L)) \end{aligned} \tag{9}$$

so

$$\begin{aligned} p_{\text{in}}(t) &= \rho_0 c_0^2 (f(c_0 t - L) + f(c_0 t + L)) \\ S_n u_n(t) &= S_b c_0 (f(c_0 t - L) - f(c_0 t + L)). \end{aligned} \tag{10}$$

After the Fourier transform of (7) using (8), we have

$$\begin{aligned} & \hat{u}(x) = Ac_0 \sin(kx + kL), && \hat{p}(x) = \mathrm{i} A \rho_0 c_0^2 \cos(kx + kL), \\ \text{hence} \quad & S_n \hat{u}_n = S_b A c_0 \sin(kL), && \hat{p}_{\text{in}} = \mathrm{i} A \rho_0 c_0^2 \cos(kL). \end{aligned}$$

For the linear harmonic case, we have from (6)

$$\mathrm{i}\omega\rho_0 \ell \hat{u}_n + R\hat{u}_n = \hat{p}_{\text{in}} - \hat{p}_{\text{ex}}, \tag{11}$$

$$\hat{p}_{\text{ex}} = -\mathrm{i}\omega\rho_0\ell \frac{S_b}{S_n} A c_0 \sin(kL) - R\frac{S_b}{S_n} A c_0 \sin(kL) + \mathrm{i} A \rho_0 c_0^2 \cos(kL). \tag{12}$$

The neck velocity $\hat{u}$ is averaged over the whole surface and can be multiplied by the porosity factor to obtain

$$\hat{u}_{\text{ex}} = \frac{S_n}{S_b}\hat{u}_n = \hat{u}(0) = Ac_0 \sin(kL). \tag{13}$$

Combining (13) with (12), we obtain the standard[1] expression of the linear impedance [16]

$$\begin{aligned} Z = \frac{\hat{p}_{\text{ex}}}{-\hat{u}_{\text{ex}}} &= \frac{-\mathrm{i}\omega\rho_0\ell\frac{S_b}{S_n} A c_0 \sin(kL) - R\frac{S_b}{S_n} A c_0 \sin(kL) + \mathrm{i} A \rho_0 c_0^2 \cos(kL)}{-Ac_0 \sin(kL)} \\ &= \frac{S_b}{S_n}(R + \mathrm{i}\omega\rho_0\ell) - \mathrm{i}\rho_0 c_0 \cot(kL). \end{aligned} \tag{14}$$

The resistance R averaged over the surface becomes the resistance term of the impedance in the linear regime. Close to resonance, the expression (14) is no longer valid because the nonlinear term in (6) is of the same order of magnitude as the other terms (the problem is formulated such that the nonlinear effects become important near resonance), as will become more clear in the next section. In order to make progress with the perturbation problem, it is essential to scale the variables in (6). This will be done in the next section.

III. Scaling

For a proper analysis, it is most clarifying to rewrite the equation into non-dimensional variables, and scaled to the right order of magnitude. For this we need an inherent timescale and pressure level. The fundamental[2] resonance frequency ω_0 for the linearised case and $R = 0$ is evidently given by the first positive solution of

$$\kappa_0 \tan \kappa_0 = \frac{LS_n}{\ell S_b}, \quad \kappa_0 = \frac{\omega_0 L}{c_0}. \tag{15}$$

The reciprocal of this angular frequency is a suitable timescale of the problem. By dividing the nonlinear damping term by the acceleration term we find the pressure level at which the

[1] Whenever convenient, we will use tan = sin / cos, cot = cos / sin, sec = 1/ cos, cosec = 1/ sin.
[2] Resonance at the higher harmonics will not be considered.

nonlinear damping would be just as large as the other terms. So for a pressure that is a small fraction, say ε, of this level we have a problem with only little nonlinear damping. In addition we assume that the linear damping is small, and (near resonance[3]) of the same order of magnitude as the nonlinear damping. As may be expected, the driving amplitude p_{ex} will (near resonance) be an order smaller than p_{in}. In order to make all this explicit we introduce a small parameter ε (via the external forcing amplitude), and make dimensionless

$$\begin{aligned} &\tau = \omega_0 t && p_{\text{in}}(t) = 2\varepsilon\rho_0 c_0^2 \left(\frac{\omega_0 \ell}{c_0}\right)^2 y(\tau) && p_{\text{ex}}(t) = 2\varepsilon^2 \rho_0 c_0^2 \left(\frac{\omega_0 \ell}{c_0}\right)^2 F(\tau) \\ &R = \varepsilon \rho_0 c_0 \left(\frac{\omega_0 \ell}{c_0}\right) r && u_{\text{n}}(t) = 2\varepsilon c_0 \left(\frac{\omega_0 \ell}{c_0}\right) v(\tau) && f(c_0 t) = 2\varepsilon \left(\frac{\omega_0 \ell}{c_0}\right)^2 \phi(\tau). \end{aligned} \tag{16}$$

It may be helpful to explicate the relation between bookkeeping parameter ε and the excitation amplitude of p_{ex}. The relation is similar to what is used in [14], only ω_0 is now found from (15). Although p_{ex} is non-dimensionalised and rescaled such that $F = O(1)$, there are many ways for F to be $O(1)$, and the precise value of ε depends therefore on the chosen normalisation of F. If we assume, for definiteness (and because this has been assumed in all the examples), that the excitation is harmonic with amplitude unity, in particular $F = \cos(\omega t)$, we can relate ε directly to the excitation *SPL* dB value by

$$\varepsilon = \left(\frac{2 \cdot 10^{-5} \cdot 10^{\frac{\text{SPL}}{20}}}{2\rho_0 c_0^2 \left(\frac{\omega_0 \ell}{c_0}\right)^2 \frac{1}{2}\sqrt{2}} \right)^{\frac{1}{2}}. \tag{17}$$

It should be noted that the modelling assumptions consider resistance parameter R a constant and not dependent of the excitation amplitude, and thus ε. So the used scaling $R \sim \varepsilon r$ should not be interpreted that R depends on ε, but is only meant to further the asymptotic analysis and select out a certain class of problems with a relatively small linear friction and nonlinear effects. If we consider a particular configuration, with fixed R, for varying excitation amplitude ($\sim \varepsilon^2$), we should keep εr fixed and adapt r accordingly. It goes without saying that r should never become so large that we enter a physically different regime.

Coupled with (6) and (9), we obtain the final nonlinear differential equation in y and v

$$\frac{\mathrm{d}v}{\mathrm{d}\tau} + \varepsilon v|v| + \varepsilon r v - y = -\varepsilon F \tag{18}$$

under the condition that there is a function ϕ with

$$\begin{aligned} \phi(\tau - \kappa_0) + \phi(\tau + \kappa_0) &= y(\tau) \\ \phi(\tau - \kappa_0) - \phi(\tau + \kappa_0) &= v(\tau) \tan \kappa_0. \end{aligned} \tag{19}$$

This condition (19) indeed simplifies for $\kappa_0 \to 0$ to the condition $v(\tau) = -y'(\tau)$, used in the analysis of [14] (in particular, equivalent to its equation (8)). Moreover, in this case we have

$$\kappa_0 \tan \kappa_0 \simeq \kappa_0^2.$$

leading, with (15), to the same resonance frequency of the cavity as in [14]. Note that with positive ω_0, $\kappa_0 > 0$, and since the product $k_0 \tan \kappa_0 = LS_n/\ell S_b > 0$, we have $\tan \kappa_0 > 0$.

This system of equations (18, 19) is to be solved asymptotically in the following.

[3] Away from resonance the nonlinear effects will be much smaller.

IV. Asymptotic solution away from resonance, ω not near ω_0

Away from resonance, $\omega \neq \omega_0$, and with F given by[4]

$$F(\tau) = F_0 \cos(\Omega\tau), \quad \Omega = \frac{\omega}{\omega_0}, \tag{20}$$

our solution y follows the external excitation εF in time, phase and order of magnitude. Hence we assume $y = O(\varepsilon)$ and expand the variables as

$$y = \varepsilon y_0 + \varepsilon^2 y_1 + \ldots, \qquad v = \varepsilon v_0 + \varepsilon^2 v_1 + \ldots, \qquad \phi = \varepsilon\phi_0 + \varepsilon^2\phi_1 + \ldots. \tag{21}$$

Collecting the like powers of ε, we obtain

$$\begin{aligned} \frac{\mathrm{d}v_0}{\mathrm{d}\tau} - y_0 &= -F_0\cos(\Omega\tau) \\ \phi_0(\tau-\kappa_0) + \phi_0(\tau+\kappa_0) &= y_0(\tau) \\ \phi_0(\tau-\kappa_0) - \phi_0(\tau+\kappa_0) &= v_0(\tau)\tan\kappa_0 \end{aligned} \tag{22}$$

and

$$\begin{aligned} \frac{\mathrm{d}v_1}{\mathrm{d}\tau} - y_1 &= -rv_0 \\ \phi_1(\tau-\kappa_0) + \phi_1(\tau+\kappa_0) &= y_1(\tau) \\ \phi_1(\tau-\kappa_0) - \phi_1(\tau+\kappa_0) &= v_1(\tau)\tan\kappa_0. \end{aligned} \tag{23}$$

Assuming a slight amount of damping, the homogeneous solution of (22) and (23), given by (70) of Appendix A, will dissipate for large time. The particular solution that remains, can be obtained in a way as shown in Appendix B. Using (73), we obtain

$$v = \varepsilon\frac{-\tan(\Omega\kappa_0)}{\Omega\tan(\Omega\kappa_0)-\tan\kappa_0}F_0\sin(\Omega\tau) - \varepsilon^2 r\left[\frac{\tan(\Omega\kappa_0)}{\Omega\tan(\Omega\kappa_0)-\tan\kappa_0}\right]^2 F_0\cos(\Omega\tau) + O(\varepsilon^3),$$

which is asymptotically equivalent to the solution

$$v = -\varepsilon F_0\tan(\Omega\kappa_0)\frac{(\Omega\tan(\Omega\kappa_0)-\tan\kappa_0)\sin(\Omega\tau) + \varepsilon r\tan(\Omega\kappa_0)\cos(\Omega\tau)}{(\Omega\tan(\Omega\kappa_0)-\tan\kappa_0)^2 + (\varepsilon r\tan(\Omega\kappa_0))^2} + O(\varepsilon^3). \tag{24}$$

We see that the response v is indeed $O(\varepsilon)$ and follows the excitation almost in phase ($\Omega\tan(\Omega\kappa_0) - \tan\kappa_0 > 0$) or antiphase ($\Omega\tan(\Omega\kappa_0) - \tan\kappa_0 < 0$).

On the other hand, close to resonance when $\Omega = 1+O(\varepsilon)$, the term $(\Omega\tan(\Omega\kappa_0)-\tan\kappa_0) = O(\varepsilon)$, so $v = O(1)$ and the assumption that the response v has the same order as the excitation $O(\epsilon)$ is not correct. Therefore the solution (24) is not valid close to resonance.

V. Asymptotic solution close to resonance, $\omega \approx \omega_0$

Near resonance, the amplitude y in (18) rises to levels of $O(1)$ with $O(\varepsilon)$ forcing and the assumption that the nonlinear damping is negligible to leading orders is not correct. As the physics of the problem essentially change when $\Omega = 1+O(\varepsilon)$, we introduce a parameter $\sigma = O(1)$ and assume that

$$\Omega = 1 + \varepsilon\sigma. \tag{25}$$

[4]We include amplitude F_0 for lucidity of the formulas, but in all examples $F_0 = 1$ will be used.

However, posed in this form we obtain secular terms in the expansion $\cos(\tau+\varepsilon\sigma\tau)=\cos(\tau)-\varepsilon\sigma\tau\sin(\tau)+\dots$ of the driving force, which prohibits a uniform approximation of v later [17, sec 15.3.2]. Therefore, we remove the ε-dependence from the driving force by absorbing Ω into a new time coordinate $\tilde\tau=\Omega\tau$. Moreover, the asymptotic expansion of the term $v|v|$ introduces difficulties near the ε-dependent (and unknown) zeros of v. This will be tackled by a translation of the origin by an amount $\theta(\varepsilon)$, such that the locations of the sign change of v are fixed (as v is synchronised with the driving force) and independent of ε. (Of course, a certain amount of smoothness is anticipated such that v has the same number of zeros per period as the forcing term). So we introduce

$$\tilde\tau=\Omega\tau-\theta(\varepsilon) \tag{26}$$

where θ is to be chosen such that the response v vanishes at integral multiples of π. This fixes the points along the time $\tilde\tau$ axis where v changes sign, *i.e.*

$$v(\tilde\tau)=0\quad\text{at}\quad\tilde\tau=N\pi. \tag{27}$$

In other words, $\Omega\tau=\omega t=\theta$ corresponds with the phase lag of response v_{ex} to excitation p_{ex} like in [14].

Consider $\Omega=1+O(\varepsilon)$ and introduce the transformation

$$F=F_0\cos(\tilde\tau+\theta),\ \Omega=1+\varepsilon\sigma,\ \tilde\tau=\Omega\tau-\theta,\ y(\tau)=\tilde y(\tilde\tau),\ v(\tau)=\tilde v(\tilde\tau)\text{ and }\phi(\tau)=\tilde\phi(\tilde\tau), \tag{28}$$

to obtain the following set of equations

$$\Omega\frac{\mathrm{d}\tilde v}{\mathrm{d}\tilde\tau}+\varepsilon\tilde v|\tilde v|+\varepsilon r\tilde v-\tilde y=-\varepsilon F \tag{29}$$

with

$$\begin{aligned}\tilde\phi(\tilde\tau-\Omega\kappa_0)+\tilde\phi(\tilde\tau+\Omega\kappa_0)&=\tilde y(\tilde\tau)\\ \tilde\phi(\tilde\tau-\Omega\kappa_0)-\tilde\phi(\tilde\tau+\Omega\kappa_0)&=\tilde v(\tilde\tau)\tan\kappa_0.\end{aligned} \tag{30}$$

Now we expand the variables as follows

$$\begin{aligned}&\tilde y=\tilde y_0+\varepsilon\tilde y_1+\dots,\quad \tilde v=\tilde v_0+\varepsilon\tilde v_1+\dots,\quad \tilde\phi=\tilde\phi_0+\varepsilon\tilde\phi_1+\dots,\quad \theta=\theta_0+\varepsilon\theta_1+\dots,\\ &\tilde\phi(\tilde\tau\pm\Omega\kappa_0)=\tilde\phi_0(\tilde\tau\pm\kappa_0)+\varepsilon(\tilde\phi_1(\tilde\tau\pm\kappa_0)\pm\sigma\kappa_0\tilde\phi_0'(\tilde\tau\pm\kappa_0))\\ &\qquad\qquad+\varepsilon^2\left[\tilde\phi_2(\tilde\tau\pm\kappa_0)\pm\sigma\kappa_0\tilde\phi_1'(\tilde\tau\pm\kappa_0)+\tfrac12(\sigma\kappa_0)^2\tilde\phi_0''(\tilde\tau\pm\kappa_0)\right]+\dots.\end{aligned} \tag{31}$$

Next we collect the terms of the same order of ε and construct our solution in the form of an asymptotic series.

Order ε^0 analysis:

Substituting (31) in (30) and afterwards in (29) and collecting the terms of $O(\varepsilon^0)$, we have

$$\begin{aligned}\frac{\mathrm{d}\tilde v_0}{\mathrm{d}\tilde\tau}-\tilde y_0&=0\\ \tilde\phi_0(\tilde\tau-\kappa_0)+\tilde\phi_0(\tilde\tau+\kappa_0)&=\tilde y_0(\tilde\tau)\\ \tilde\phi_0(\tilde\tau-\kappa_0)-\tilde\phi_0(\tilde\tau+\kappa_0)&=\tilde v_0(\tilde\tau)\tan\kappa_0.\end{aligned} \tag{32}$$

At large times, assuming a little damping, the cavity is driven by the external force in such a way that a steady state is reached and the initial conditions are not important. Hence from (70), we choose the steady solution and obtain, using (27),

$$\tilde\phi_0=\tfrac12 A_0\cos\tilde\tau, \tag{33}$$

and hence

$$\tilde{y}_0 = A_0 \cos\kappa_0 \cos\tilde{\tau} \quad \text{and} \quad \tilde{v}_0 = A_0 \cos\kappa_0 \sin\tilde{\tau}, \tag{34}$$

where A_0 and θ_0 are to be determined from the regularity condition (absence of secular terms (74)) in the next order ε^1.

Order ε^1 analysis:

Collecting the terms of $O(\varepsilon)$ from (29), we obtain

$$\begin{aligned}
\frac{\mathrm{d}\tilde{v}_1}{\mathrm{d}\tilde{\tau}} - \tilde{y}_1 &= -\sigma\tilde{v}_0' - \tilde{v}_0|\tilde{v}_0| - r\tilde{v}_0 - F_0\cos(\tilde{\tau}+\theta_0) \\
\tilde{\phi}_1(\tilde{\tau}-\kappa_0) + \tilde{\phi}_1(\tilde{\tau}+\kappa_0) &= \sigma\kappa_0\tilde{\phi}_0'(\tilde{\tau}-\kappa_0) - \sigma\kappa_0\tilde{\phi}_0'(\tilde{\tau}+\kappa_0) + \tilde{y}_1(\tilde{\tau}) \\
\tilde{\phi}_1(\tilde{\tau}-\kappa_0) - \tilde{\phi}_1(\tilde{\tau}+\kappa_0) &= \sigma\kappa_0\tilde{\phi}_0'(\tilde{\tau}-\kappa_0) + \sigma\kappa_0\tilde{\phi}_0'(\tilde{\tau}+\kappa_0) + \tilde{v}_1(\tilde{\tau})\tan\kappa_0.
\end{aligned} \tag{35}$$

From (33), (34) and (35), we have after eliminating $\tilde{y}_1$ and $\tilde{v}_1$

$$\begin{aligned}
\cot\kappa_0 \left[\tilde{\phi}_1'(\tilde{\tau}-\kappa_0) - \tilde{\phi}_1'(\tilde{\tau}+\kappa_0)\right] - \left[\tilde{\phi}_1(\tilde{\tau}-\kappa_0) + \tilde{\phi}_1(\tilde{\tau}+\kappa_0)\right] = \\
- \sigma A_0\left[1 + 2\kappa_0\cot(2\kappa_0)\right]\cos\kappa_0\cos\tilde{\tau} - A_0|A_0|\cos^2\kappa_0\sin\tilde{\tau}|\sin\tilde{\tau}| \\
- rA_0\cos\kappa_0\sin\tilde{\tau} - F_0\cos\theta_0\cos\tilde{\tau} + F_0\sin\theta_0\sin\tilde{\tau}.
\end{aligned} \tag{36}$$

From the argument, that we have a stationary solution of which we require its asymptotic expansion uniform in $\tilde{\tau}$, it follows that no resonant excitation is allowed in the right hand side of the equation (36) (no secular terms). This means (see (74)) that we should suppress the sine and cosine terms including those in the Fourier expansion of

$$\sin(x)|\sin(x)| = -\frac{1}{\pi}\sum_{n=0}^{\infty}\frac{\sin(2n+1)x}{(n^2-\frac{1}{4})(n+\frac{3}{2})} \sim \frac{8}{3\pi}\sin(x) - \frac{8}{15\pi}\sin(3x) - \ldots.$$

Hence we obtain the algebraic equations

$$\begin{aligned}
F_0\cos\theta_0 &= -\sigma A_0\left[1 + 2\kappa_0\cot(2\kappa_0)\right]\cos\kappa_0 \\
F_0\sin\theta_0 &= A_0\left[r + \frac{8}{3\pi}|A_0|\cos\kappa_0\right]\cos\kappa_0.
\end{aligned} \tag{37}$$

In general, A_0 has to be solved numerically, from which θ_0 follows. There exist two (real) solutions, but they are equivalent. If (A_0, θ_0) is a solution, then also $(-A_0, \theta_0+\pi)$. For convenience, we will assume that θ_0 is taken such that A_0 is positive and maintain $|A_0| = A_0$. Solving (37), we can obtain A_0 and θ_0 as plotted in Fig. 3. We notice that the amplitude rises to $O(1)$ at resonance and decays when $\sigma \to \pm\infty$.

If we take the low frequency limit ($\kappa_0 \to 0$) in (37), we obtain exactly the same equations as in [14]. Physically, in this limit, the cavity length L would be asymptotically much smaller than the acoustic wavelength $2\pi c_0/\omega_0$ and hence the wave would feel a uniform pressure inside the cavity. Thus the current modelling assumption converges to the one in [14].

From (36), we have

$$\cot\kappa_0\left[\tilde{\phi}_1'(\tilde{\tau}-\kappa_0) - \tilde{\phi}_1'(\tilde{\tau}+\kappa_0)\right] - \left[\tilde{\phi}_1(\tilde{\tau}-\kappa_0) + \tilde{\phi}_1(\tilde{\tau}+\kappa_0)\right] = \frac{1}{\pi}A_0^2\cos^2\kappa_0\sum_{n=1}^{\infty}\frac{\sin(2n+1)\tilde{\tau}}{(n^2-\frac{1}{4})(n+\frac{3}{2})}$$

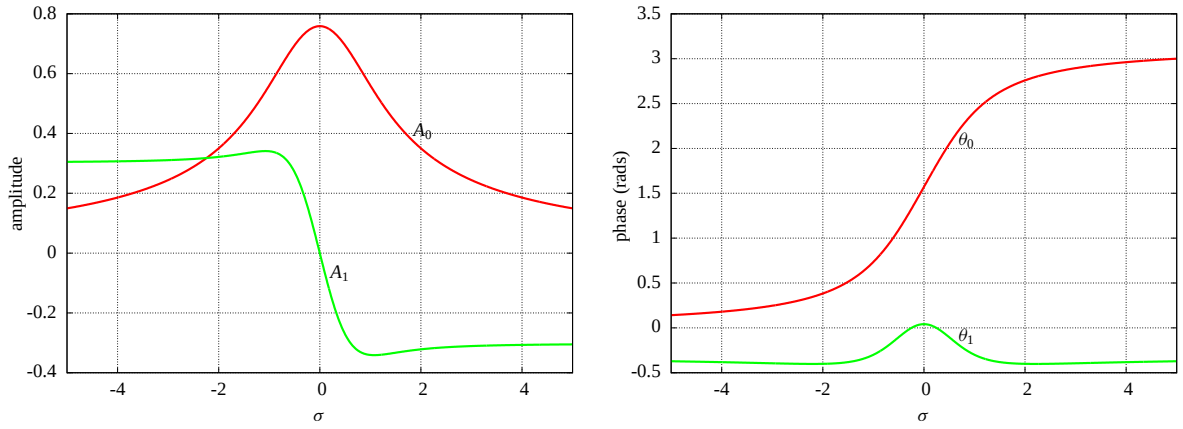

Figure 3. Solution of amplitude (A_0, A_1) and phase (θ_0, θ_1) as a function of σ, with $\kappa_0 = 0.55$, and $r = F_0 = 1$

which can be solved term-wise using (70), similar to (33), to obtain

$$\tilde{\phi}_1(\tilde{\tau}) = \tfrac{1}{2}A_1 \cos\tilde{\tau} + \tfrac{1}{2}B_1 \sin\tilde{\tau} + \frac{1}{2\pi}A_0^2 \cos\kappa_0 \sum_{n=1}^{\infty} \frac{\sin(2n+1)\tilde{\tau}}{(n^2-\frac{1}{4})(n+\frac{3}{2})\left[2n+1-\tan\kappa_0\cot(2n+1)\kappa_0\right]} \cdot \frac{\sin\kappa_0}{\sin(2n+1)\kappa_0} \tag{38}$$

which upon substituting in (35) gives

$$\tilde{v}_1(\tilde{\tau}) = \Bigg[A_1 \sin\tilde{\tau} - B_1\cos\tilde{\tau} + \sigma A_0\kappa_0 \cot\kappa_0 \sin\tilde{\tau} - \frac{1}{\pi}A_0^2\cos\kappa_0 \sum_{n=1}^{\infty} \frac{\cos(2n+1)\tilde{\tau}}{(n^2-\frac{1}{4})(n+\frac{3}{2})\left[2n+1-\tan\kappa_0\cot(2n+1)\kappa_0\right]}\Bigg] \cos\kappa_0. \tag{39}$$

Using the condition (27), *i.e.* $\tilde{v}_1(\tilde{\tau} = N\pi) = 0$, we find

$$B_1 = -\frac{1}{\pi}A_0^2 \cos\kappa_0 \sum_{n=1}^{\infty} \frac{1}{(n^2-\frac{1}{4})(n+\frac{3}{2})\left[2n+1-\tan\kappa_0\cot(2n+1)\kappa_0\right]}. \tag{40}$$

Note that in the limit $\kappa_0 \to 0$, we have $B_1 = -\frac{2}{9\pi}A_0^2$, which will be useful later[5]. The other two unknowns A_1 and θ_1 are to be determined from the regularity condition at next order (ε^2).

Order ε^2 analysis:

Collecting the terms of $O(\varepsilon^2)$ from (29), we obtain

$$\begin{aligned}
\tilde{v}_2' - \tilde{y}_2 &= -\sigma\tilde{v}_1' - 2\tilde{v}_1|\tilde{v}_0| - r\tilde{v}_1 + \theta_1\sin(\tilde{\tau}+\theta_0) \\
\tilde{\phi}_2(\tilde{\tau}-\kappa_0) + \tilde{\phi}_2(\tilde{\tau}+\kappa_0) &= -\tfrac{1}{2}(\sigma\kappa_0)^2\left[\tilde{\phi}_0''(\tilde{\tau}-\kappa_0) + \tilde{\phi}_0''(\tilde{\tau}+\kappa_0)\right] \\
&\quad + \sigma\kappa_0\left[\tilde{\phi}_1'(\tilde{\tau}-\kappa_0) - \tilde{\phi}_1'(\tilde{\tau}+\kappa_0)\right] + \tilde{y}_2(\tilde{\tau}) \\
\tilde{\phi}_2(\tilde{\tau}-\kappa_0) - \tilde{\phi}_2(\tilde{\tau}+\kappa_0) &= -\tfrac{1}{2}(\sigma\kappa_0)^2\left[\tilde{\phi}_0''(\tilde{\tau}-\kappa_0) - \tilde{\phi}_0''(\tilde{\tau}+\kappa_0)\right] \\
&\quad + \sigma\kappa_0\left[\tilde{\phi}_1'(\tilde{\tau}-\kappa_0) + \tilde{\phi}_1'(\tilde{\tau}+\kappa_0)\right] + \tilde{v}_2(\tilde{\tau})\tan\kappa_0.
\end{aligned} \tag{41}$$

[5]The series of B_1 breaks down at the zeros of $2n+1-\tan\kappa_0\cot(2n+1)\kappa_0$, and so the smoothness properties in variable κ_0 of B_1, and for that matter of $\tilde{\phi}_1$ and $\tilde{v}_1$, are still a point of attention. The issue is directly related to the modelling assumptions leading to the term $u_n|u_n|$ in (6).

Substituting $\tilde{y}_2$ and $\tilde{v}_2$ in the first equation of (41), we obtain

$$\begin{aligned}\cot\kappa_0\left[\tilde{\phi}_2'(\tilde{\tau}-\kappa_0)-\tilde{\phi}_2'(\tilde{\tau}+\kappa_0)\right]-\left[\tilde{\phi}_2(\tilde{\tau}-\kappa_0)+\tilde{\phi}_2(\tilde{\tau}+\kappa_0)\right]=\\ \tfrac{1}{2}(\sigma\kappa_0)^2\left[\tilde{\phi}_0''(\tilde{\tau}-\kappa_0)+\tilde{\phi}_0''(\tilde{\tau}+\kappa_0)\right]-\tfrac{1}{2}(\sigma\kappa_0)^2\cot\kappa_0\left[\tilde{\phi}_0'''(\tilde{\tau}-\kappa_0)-\tilde{\phi}_0'''(\tilde{\tau}+\kappa_0)\right]\\ -\sigma\kappa_0\left[\tilde{\phi}_1'(\tilde{\tau}-\kappa_0)-\tilde{\phi}_1'(\tilde{\tau}+\kappa_0)\right]+\sigma\kappa_0\cot\kappa_0\left[\tilde{\phi}_1''(\tilde{\tau}-\kappa_0)+\tilde{\phi}_1''(\tilde{\tau}+\kappa_0)\right]\\ -\sigma\tilde{v}_1'-2\tilde{v}_1|\tilde{v}_0|-r\tilde{v}_1+\theta_1\sin(\tilde{\tau}+\theta_0),\end{aligned}\tag{42}$$

in which we have to suppress the sine and cosine terms to obtain A_1 and θ_1. Although laborious, this is simple. By using (33), (34), (38), (39) and (40) with (42), (see Appendix C), collecting the coefficients of sine and cosine terms, and equating them to zero, we obtain two linear equations in the variables A_1 and θ_1

$$\begin{aligned}&\sigma\left[1+2\kappa_0\operatorname{cosec}(2\kappa_0)\right]A_1\cos\kappa_0-\theta_1\sin\theta_0=\\ &\qquad\left(r+\frac{8}{3\pi}A_0\cos\kappa_0\right)B_1\cos\kappa_0-\sigma^2A_0\kappa_0\cot\kappa_0\cos\kappa_0\\ &\qquad-\frac{2}{\pi^2}A_0^3\cos^3\kappa_0\sum_{n=1}^{\infty}\frac{1}{(n-\frac{1}{2})(n^2-\frac{1}{4})(n+\frac{3}{2})^2\left[2n+1-\tan\kappa_0\cot(2n+1)\kappa_0\right]}\\ &\left(r+\frac{16}{3\pi}A_0\cos\kappa_0\right)A_1\cos\kappa_0-\theta_1\cos\theta_0=\\ &\qquad-\sigma\left[1+2\kappa_0\operatorname{cosec}(2\kappa_0)\right]B_1\cos\kappa_0-\sigma\left(r+\frac{16}{3\pi}A_0\cos\kappa_0\right)A_0\kappa_0\cot\kappa_0\cos\kappa_0.\end{aligned}\tag{43}$$

Solving (43) is straightforward. An example of the found A_1 and θ_1 is shown in Fig. 3. At this stage we have the solution correct up to $O(\varepsilon)$. To verify the consistency with the simpler model [14], it is of interest to consider the limit $\kappa_0\to 0$. By noting that

$$\sum_{n=1}^{\infty}\frac{2n+1}{4n(n+1)(n-\frac{1}{2})(n^2-\frac{1}{4})(n+\frac{3}{2})^2}=\frac{\pi^2}{6}-\frac{40}{27},$$

we obtain from (43) for $\kappa_0\to 0$

$$\begin{aligned}2\sigma A_1-\theta_1\sin\theta_0&=-\sigma^2A_0-\frac{2}{9\pi}rA_0^2-\frac{1}{3}\left(1-\frac{64}{9\pi^2}\right)A_0^3\\ \left(r+\frac{16}{3\pi}A_0\right)A_1-\theta_1\cos\theta_0&=-\sigma\left(r+\frac{44}{9\pi}A_0\right)A_0\end{aligned}\tag{44}$$

which is indeed exactly the equation set of [14]. This confirms the consistency between current and previous solutions. Using (39), (31), (28) and (16), we finally obtain

$$\begin{aligned}u_n=&2\varepsilon\ell\omega_0\cos\kappa_0\left[(A_0+\varepsilon A_1+\varepsilon\sigma A_0\kappa_0\cot\kappa_0)\sin(\omega t-\theta)-\varepsilon B_1\cos(\omega t-\theta)\right]\\ &-2\varepsilon^2\frac{\ell\omega_0}{\pi}A_0^2\cos^2\kappa_0\sum_{n=1}^{\infty}\frac{\cos(2n+1)(\omega t-\theta)}{(n^2-\frac{1}{4})(n+\frac{3}{2})\left(2n+1-\tan\kappa_0\cot(2n+1)\kappa_0\right)}.\end{aligned}\tag{45}$$

The velocity in (45) after averaging over the surface (multiplying with S_n/S_b) can be used with the external excitation in (16) to obtain the impedance that we will derive in the next section. It is interesting to note that equation (45) reduces to leading order in ε and vanishing κ_0 to

$$u_n(t)=2\varepsilon\ell\omega_0A_0\cos\kappa_0\sin(\omega t-\theta_0)\simeq 2\varepsilon\ell\omega_0A_0\sin(\omega t-\theta_0),\tag{46}$$

which is almost the same as the corresponding expression in [14]. The only difference is the factor ω_0 here, versus the factor ω in the previous solution. This, however, is not an error, since near resonance $\Omega = \omega/\omega_0 \approx 1$, and ω and ω_0 are asymptotically equivalent. Via another route we would have found the factor ω here too. If we expand the function $\tilde{\phi}(\tilde{\tau} - \Omega\kappa_0)$ about $\Omega\kappa_0$ in (30) assuming small κ_0, we obtain

$$\tilde{y}(\tilde{\tau}) = 2\tilde{\phi}(\tilde{\tau}) \quad \text{and} \quad \tilde{v}(\tilde{\tau}) = -2\Omega\tilde{\phi}'(\tilde{\tau}), \quad (\text{and hence} \quad \tilde{v} = -\Omega\tilde{y}',) \tag{47}$$

that can be substituted back in (29) to obtain

$$\Omega^2\tilde{y}''(\tilde{\tau}) + \varepsilon\Omega^2\tilde{y}'(\tilde{\tau})|\tilde{y}'(\tilde{\tau})| + \varepsilon\Omega r\tilde{y}'(\tilde{\tau}) + \tilde{y}(\tilde{\tau}) = \varepsilon F. \tag{48}$$

This is exactly the equation analysed by [14] in the nonlinear regime, while $\tilde{v} = -\Omega\tilde{y}'$ comes down dimensionally to the condition

$$V\frac{\mathrm{d}p_{\mathrm{in}}}{\mathrm{d}t} = -\rho_0 c_0^2 u_n S_n, \tag{49}$$

with $V = S_b L$ the volume of the cavity. From (34) and (16), we obtain

$$p_{\mathrm{in}}(t) = 2\varepsilon\rho_0\ell^2\omega_0^2 A_0\cos(\omega t - \theta_0) \tag{50}$$

which upon substituting in (49) gives the alternative of (46)

$$u_n(t) = 2\varepsilon\omega\ell A_0\sin(\omega t - \theta_0). \tag{51}$$

As explained above, this difference is correct, because close to resonance ω and ω_0 are asymptotically equivalent, and so the old and new expressions are asymptotically equivalent. Nevertheless, the accidentally found difference is very interesting, because it appears that the new version happens to behave far better for *finite* values of ε. Although we cannot expect a priori an asymptotic analysis for $\varepsilon \to 0$ to produce good behaviour for finite ε, it is a fortuitous occasion if we have one.

VI. Impedance calculation

In order to obtain realistic numbers, we will consider the impedance Z as the effective impedance of an array of Helmholtz resonators, where the spatially averaged neck velocity is identified to the external acoustic velocity. Therefore, we add a porosity factor S_n/S_b to u_n and obtain

$$u_{\mathrm{ex}} = \frac{S_n}{S_b}u_n. \tag{52}$$

Then we define the impedance as the ratio of the Fourier transforms of the external pressure p_{ex} and (minus) the external velocity v_{ex} at excitation frequency ω.

$$Z(\eta) = \frac{\hat{p}_{\mathrm{ex}}(\eta)}{-\hat{u}_{\mathrm{ex}}(\eta)} = \frac{\dfrac{1}{2\pi}\displaystyle\int_{-\infty}^{\infty} p_{\mathrm{ex}}(t)\,\mathrm{e}^{-\mathrm{i}\eta t}\,\mathrm{d}t}{-\dfrac{1}{2\pi}\displaystyle\int_{-\infty}^{\infty} u_{\mathrm{ex}}(t)\,\mathrm{e}^{-\mathrm{i}\eta t}\,\mathrm{d}t} \quad (\eta = \omega). \tag{53}$$

VI.A. Non-resonant impedance

Taking the Fourier transformation of $p_{\rm ex}(t)$ from (16) with (20) and Fourier transformation of $u_{\rm ex}(t) = (S_n/S_b)u_{\rm n}(t)$ from (24), we obtain for $\eta > 0$,

$$\begin{aligned}\hat{p}_{\rm ex}(\eta) =& \frac{1}{2\pi}\int_{-\infty}^{\infty} p_{\rm ex}(t)\,{\rm e}^{-{\rm i}\eta t}\,{\rm d}t = \frac{1}{2\pi}\varepsilon^2\rho_0\ell^2\omega_0^2\,F_0\delta(\eta-\omega)\\ \hat{u}_{\rm ex}(\eta) =& \frac{1}{2\pi}\int_{-\infty}^{\infty} u_{\rm ex}(t)\,{\rm e}^{-{\rm i}\eta t}\,{\rm d}t\\ =& \frac{1}{2\pi}\frac{S_n}{S_b}\varepsilon^2\omega_0\ell\left[\frac{{\rm i}\tan(\Omega\kappa_0)}{\Omega\tan(\Omega\kappa_0)-\tan\kappa_0} - \varepsilon r\left(\frac{\tan(\Omega\kappa_0)}{\Omega\tan(\Omega\kappa_0)-\tan\kappa_0}\right)^2\right]\delta(\eta-\omega)\end{aligned} \tag{54}$$

with the negative of the ratio of above two expressions being the impedance, given by

$$Z(\omega) = \frac{S_b}{S_n}\rho_0\ell\omega_0\left[\frac{-{\rm i}\tan(\Omega\kappa_0)}{\Omega\tan(\Omega\kappa_0)-\tan\kappa_0} + \varepsilon r\left(\frac{\tan(\Omega\kappa_0)}{\Omega\tan(\Omega\kappa_0)-\tan\kappa_0}\right)^2\right]^{-1}. \tag{55}$$

To leading orders in ε, the impedance expression in (55) indeed becomes the one in (14) as expected.

VI.B. Resonant impedance

Taking the Fourier transformation of $p_{\rm ex}(t)$ from (16) with (20) and Fourier transformation of $u_{\rm ex}(t) = (S_n/S_b)u_{\rm n}(t)$ from (45), we have for $\eta > 0$

$$\hat{p}_{\rm ex}(\eta) = \frac{1}{2\pi}\int_{-\infty}^{\infty} p_{\rm ex}(t)\,{\rm e}^{-{\rm i}\eta t}\,{\rm d}t = \frac{1}{2\pi}\varepsilon^2\rho_0\ell^2\omega_0^2\,F_0\delta(\eta-\omega), \tag{56}$$

$$\begin{aligned}\hat{u}_{\rm ex}(\eta) =& \frac{1}{2\pi}\int_{-\infty}^{\infty} u_{\rm ex}(t)\,{\rm e}^{-{\rm i}\eta t}\,{\rm d}t\\ =& \frac{-{\rm i}}{2\pi}\frac{S_n}{S_b}\varepsilon\omega_0\ell\,{\rm e}^{-{\rm i}\theta}\cos\kappa_0\,[A_0+\varepsilon A_1+\varepsilon\sigma A_0\kappa_0\cot\kappa_0-{\rm i}\varepsilon B_1]\,\delta(\eta-\omega).\end{aligned} \tag{57}$$

Substituting (56) and (57) in (53), we obtain

$$Z(\omega) = \varepsilon\rho_0\ell\omega_0\frac{S_b}{S_n}\frac{-{\rm i}\,{\rm e}^{{\rm i}\theta}F_0}{A_0\cos\kappa_0+\varepsilon(A_1+\sigma A_0\kappa_0\cot\kappa_0-{\rm i}B_1)\cos\kappa_0}. \tag{58}$$

In order to illustrate formula (58), we have plotted in Fig. 4 nondimensional resistance ${\rm Re}(Z)/\rho_0 c_0$ and reactance ${\rm Im}(Z)/\rho_0 c_0$ as a function of Ω, obtained for a typical geometry at different driving amplitudes, corresponding with ε varying from 0.04 to 0.22. As may be expected from (58), the main effect of the forcing amplitude is in the resistance. The reactance is practically independent of it. Typically, the resistance increases everywhere with the amplitude, being highest at or near the resonance frequency and decaying along both sides, but more for frequencies less than the resonance frequency. Away from the resonance, if we take the limit $\sigma \to \pm\infty$, in (58), we obtain the linear impedance described by (14). Hence, the nonlinear impedance matches asymptotically to the linear impedance which confirms the consistency of our nonlinear solution.

VI.B.1. Effect of second order approximation and organ pipe cavity on the resistance

In order to understand the effect of the second order approximation on the resistance, the resistances obtained from the first ($\tilde{v}_0$) and second ($\tilde{v}_0 + \varepsilon\tilde{v}_1$) order approximations are shown in Fig. 5 *(left)*. As we can see, the second order correction is not necessary for lower driving amplitudes. For higher amplitudes, on the other hand, it is essential.

[7] Note: since $R \sim \varepsilon r$ is normally fixed, r is adapted such that εr is kept fixed.

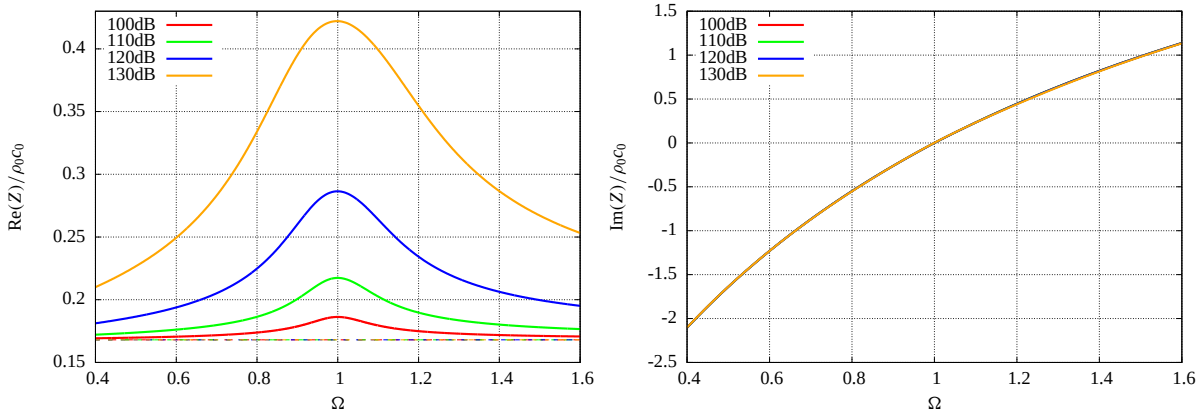

p_{ex} (dB)	100	110	120	130
ε	0.0396	0.0703	0.1251	0.2224

Figure 4. Real and imaginary parts of nondimensional impedance $Z/\rho_0 c_0$ for a finite-length Helmholtz resonator as a function of nondimensional frequency at different driving amplitudes. The realistic configuration that is chosen corresponds with $c_0 = 340\,\mathbf{m/s}$, $\rho_0 = 1.225\ \mathbf{kg/m^3}$, $\ell = 0.005\,\mathbf{m}$, $L = 0.035\,\mathbf{m}$, $R = 3.5\,\mathbf{kg/m^2 s}$ and $S_n/S_b = 0.05$, yielding $\kappa_0 = 0.5592$ and $\omega_0 = 5433$ rad/sec, while $F_0 = 1$. The dashed line along $\mathrm{Re}(Z)/\rho_0 c_0 = 0.17$ represents the linear resistance[7] which equals $(S_b/S_n)R/\rho_0 c_0$.

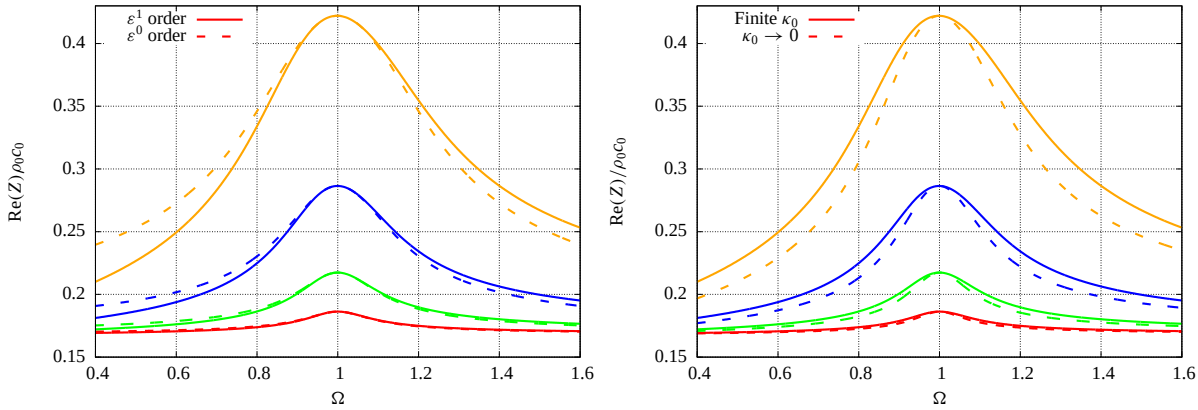

Figure 5. Nondimensional resistance, $\mathrm{Re}(Z)/\rho_0 c_0$ as a function of nondimensional frequency at different driving amplitudes. The configuration of the resonator and driving amplitudes are the same as in Fig. 4

In order to understand the effect of the organ pipe type cavity on the resistance term, we take the limit $\kappa_0 \to 0$ in (58) and obtain the expression

$$\begin{aligned} Z(\omega) &\sim \varepsilon\rho_0\ell\omega_0 \frac{S_b}{S_n} \frac{-\mathrm{i}\,\mathrm{e}^{\mathrm{i}\theta} F_0}{A_0 + \varepsilon A_1 + \varepsilon(\sigma + \mathrm{i}\frac{2}{9\pi}A_0)A_0} \\ &= \frac{\varepsilon\rho_0 c_0^2 F_0}{L\omega_0} \frac{-\mathrm{i}\,\mathrm{e}^{\mathrm{i}\theta}}{(1+\varepsilon\sigma)A_0 + \varepsilon A_1 + \mathrm{i}\varepsilon\frac{2}{9\pi}A_0^2}. \end{aligned} \tag{59}$$

The plots of resistance obtained with finite κ_0 (58) and $\kappa_0 \to 0$ (59) are shown in Fig. 5 *(right)*. For very low amplitudes (low ε), this effect is minor, but it is quite essential for higher amplitudes. Also, we notice that a finite κ_0 resistance curve has a better behaviour away from the resonance frequency when compared with the experimental data curve in Fig. 7.

VI.B.2. Comparison with previous model [14]

In view of $\omega = \omega_0(1+\varepsilon\sigma)$ and in agreement with our previous checks, the impedance expression, found by [14],

$$\begin{aligned} Z(\omega) &= \frac{\varepsilon\rho_0 c_0^2 F_0}{L\omega} \frac{-\mathrm{i}\,\mathrm{e}^{\mathrm{i}\theta}}{A_0 + \varepsilon A_1 + \mathrm{i}\varepsilon\frac{2}{9\pi}A_0^2} \\ &= \frac{\varepsilon\rho_0 c_0^2 F_0}{L\omega_0} \frac{-\mathrm{i}\,\mathrm{e}^{\mathrm{i}\theta}}{(1+\varepsilon\sigma)A_0 + (1+\varepsilon\sigma)(\varepsilon A_1 + \mathrm{i}\varepsilon\frac{2}{9\pi}A_0^2)}, \end{aligned} \tag{60}$$

is asymptotically equivalent, up to $O(\varepsilon^2)$, to (59). Asymptotically equivalent for *small* ε, however, does not automatically imply[8] equivalent for *finite* ε. Just by chance the new representation (59) behaves for finite ε much better than the previous one (60).

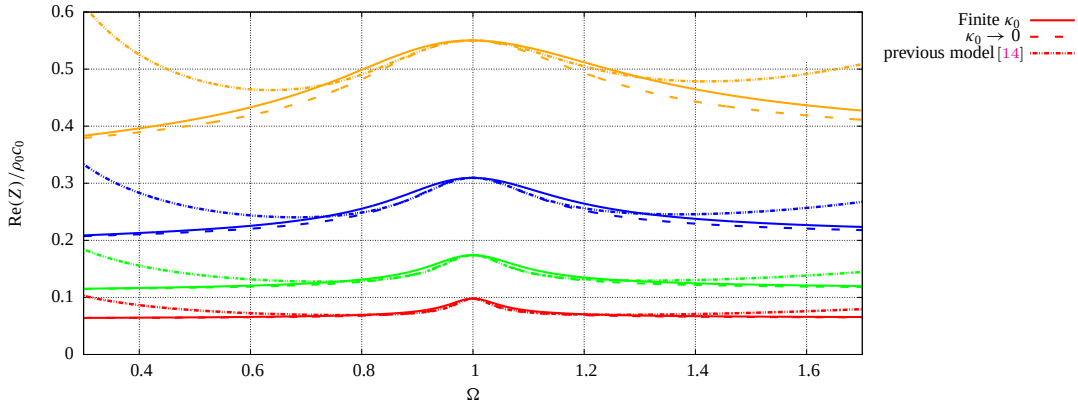

Figure 6. Comparison of nondimensional resistance $\mathrm{Re}(Z)/\rho_0 c_0$ based on the full current model, its limit for $\kappa_0 \to 0$, and (the asymptotically equivalent) [14], as a function of nondimensional frequency at different driving amplitudes. The configuration of the resonator and driving amplitudes are the same as in Fig. 4, except that $r = 1$ is kept constant

Consider Fig. 6 with a plot of the resistance obtained from (60), (58) and (59), for a typical geometry and external excitation, varying from 100 dB to 130 dB and the resistance factor $r = 1$. The current model with finite κ_0 (58) indeed predicts the near resonance behaviour to a better accuracy and decays away from resonance at $\Omega = 1$ to match with the linear resistance. Its limiting form for $\kappa_0 \to 0$, given by (59), follows the same. The near resonance behaviour (60) of [14], however, is similar to the above, but with higher ε and away from the resonance, the resistance does not decay. As said before, it turns out that (59), although asymptotically equivalent to (60), gives far better predictions at finite ε.

Hence, as a concluding remark, we suggest to replace the impedance expression derived in [14], *i.e.* (60), by the asymptotically equivalent form (59).

VII. Comparison with Motsinger and Kraft [6]

The behaviour in (58) may be compared in Fig. 7 (solid lines) with the measurements (squares) and predictions (dotted lines) given by Motsinger and Kraft in [6]. Their predictions are (a.o.) based on a resistance of the form $R = \rho_0 c_0(a + b|v|)$ with suitably chosen - and problem dependent - a and b (while $|v|$ denotes in [6] the rms-value of v). The parameter values we used are based on $c_0 = 340\,\mathrm{m/s}$, $\rho_0 = 1.225\,\mathrm{kg/m^3}$, $\omega_0/2\pi = 2210\,\mathrm{Hz}$, $\ell = 0.0017\,\mathrm{m}$, $L = 0.014\,\mathrm{m}$, $S_n/S_b = 0.0446$ and $\kappa_0 = 0.5715$. The resistance term $R = 2.25$ is deduced from the level of

[8] For example, $1 - \varepsilon = (1+\varepsilon)^{-1} + O(\varepsilon^2)$.

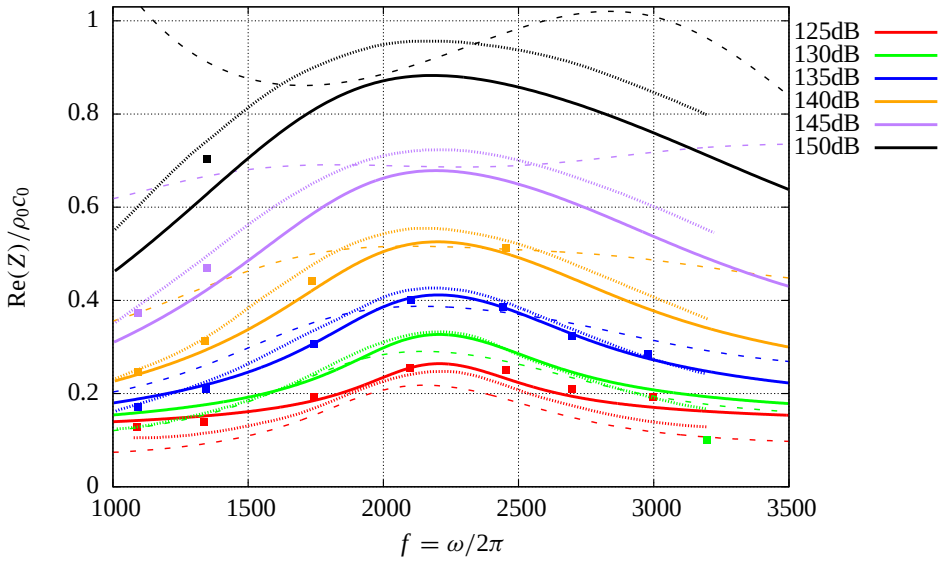

p_{ex} (dB)	125	130	135	140	145	150
ε	0.1358	0.1811	0.2415	0.3220	0.4294	0.5726

Figure 7. Comparison of (58) with measurements (squares) and predictions (dotted lines) of $\mathrm{Re}(Z)/\rho_0 c_0$ given by Motsinger and Kraft in [6]. The solid lines corresponds to the resistance values produced by (58) while the dashed lines corresponds to the previous model [14] prediction. $c_0 = 340\,\mathbf{m/s}$, $\rho_0 = 1.225\,\mathbf{m/kg^3}$, $L = 0.014\,\mathbf{m}$, $\ell = 0.0017\,\mathbf{m}$, $S_n/S_b = 0.0446$, $\kappa_0 = 0.5715$, $\omega_0/2\pi = 2210$ **Hz**

about 0.12, read off Fig. 7 in the (assumed linear) region near 1000 Hz. Applying (14), this is set equal to $(S_b/S_n)R/\rho_0 c_0$, from which follows $R = 0.12\rho_0 c_0 S_n/S_b = 2.25$. Unfortunately, only little experimental data for the higher amplitudes are available. However, the agreement is remarkably good, even when ε is relatively large for higher amplitudes. The impedance for higher amplitudes ($\sim \varepsilon^2$) at and near resonance is predicted much more accurately compared to the previous model, which is plotted by dashed lines. So we conclude that the current model has indeed a better accuracy and could be used to predict the impedance for resonators of small or big lengths.

VIII. Conclusions

A systematic approximation of the hydrodynamically nonlinear Helmholtz resonator equation that includes higher order axial modes in the cavity is obtained, including the resulting impedance if the resonator as applied in an acoustic liner. The only unknown parameters that we need to adapt is resistance factor r, and to a certain extent the effective neck length ℓ and neck cross section S_n. Comparisons with measurements show that the model predicts the near resonance impedance behaviour at $\sigma = O(1)$ to a good accuracy and a better resemblance is found (especially for higher excitation amplitudes) compared to the previous model [14]. The real part of the found impedance (the resistance) shows the usual characteristic behaviour as a function of frequency, namely a maximum at the resonance frequency and a decay along both sides. All values increase with the amplitude. The imaginary part of the impedance (the reactance) is linear in frequency in a way that it vanishes at resonance and is practically independent of the amplitude. The nonlinear solution asymptotically matches smoothly with the linear solution, which confirms the consistency of our solution.

Acknowledgement

A first draft of this work was presented at the 22nd AIAA/CEAS Aeroacoustics Conference, Lyon, France, as paper AIAA-2016-2887, entitled "*An Asymptotic Model for Non-linear Helmholtz Resonator of Finite Depth*".

We gratefully acknowledge the support from the European Union through ITN-project *FlowAirS* (contract no. FP7-PEOPLE-2011-ITN-289352), with co-ordinator Yves Aurégan.

A. Solution of homogeneous problem

Consider the homogeneous equation

$$\begin{aligned} \frac{\mathrm{d}v}{\mathrm{d}\tau} - y &= 0 \\ \phi(\tau-\kappa_0) + \phi(\tau+\kappa_0) &= y(\tau) \\ \phi(\tau-\kappa_0) - \phi(\tau+\kappa_0) &= v(\tau)\tan\kappa_0. \end{aligned} \tag{61}$$

Assume for the homogeneous problem the trial solutions

$$y = A\,\mathrm{e}^{\mathrm{i}\lambda\tau}, \quad v = B\,\mathrm{e}^{\mathrm{i}\lambda\tau}, \quad \phi = C\,\mathrm{e}^{\mathrm{i}\lambda\tau}. \tag{62}$$

Substituting (62) back into (61), we find

$$2C\cos(\lambda\kappa_0) = A = \mathrm{i}\lambda B, \quad -2\mathrm{i}C\sin(\lambda\kappa_0) = B\tan\kappa_0, \tag{63}$$

leading to

$$\lambda\tan(\lambda\kappa_0) = \tan\kappa_0. \tag{64}$$

All solutions of (64) come in pairs. If λ is solution then $-\lambda$ is also a solution. However from (15), we notice that for a positive ω_0, $\kappa_0 >$ and since product $\kappa_0\tan\kappa_0 = LS_n/\ell S_b$ is a positive constant, $\tan\kappa_0 < 0$ does not occur. For $\tan\kappa_0 > 0$, λ is given as

$$\lambda_1 = 1, \quad \lambda_2, \quad \lambda_3, \ldots. \tag{65}$$

For example: if $\kappa_0 = \frac{1}{4}\pi$ and $\tan\kappa_0 = 1$, then

$$\lambda_1 = 1, \quad \lambda_2 = 4.291488, \quad \lambda_3 = 8.1553478 \quad \text{etc.} \tag{66}$$

So the general solution for $\tan\kappa_0 > 0$ is[9]

$$y = a_1\cos\tau + b_1\sin\tau + \sum_{n=2}^{\infty} a_n\cos(\lambda_n\tau) + b_n\sin(\lambda_n\tau). \tag{70}$$

[9] Although it is not relevant here, if $\tan\kappa_0 < 0$, λ is given by

$$\lambda_0 = \mathrm{i}\mu_0, \quad \mu_0\tanh(\mu_0\kappa_0) = -\tan\kappa_0, \quad \lambda_1 = 1, \quad \lambda_2, \ldots. \tag{67}$$

For example, if $\kappa_0 = \frac{3}{4}\pi$ and $\tan\kappa_0 = -1$,

$$\lambda_0 = \mathrm{i}1.016743, \quad \lambda_1 = 1, \quad \lambda_2 = 2.505496, \quad \lambda_3 = 3.893295, \quad \lambda_4 = 5.253502 \quad \text{etc.} \tag{68}$$

So for $\tan\kappa_0 < 0$, with the presence of diverging exponential terms,

$$y = a_0\,\mathrm{e}^{\mu_0\tau} + b_0\,\mathrm{e}^{-\mu_0\tau} + a_1\cos\tau + b_1\sin\tau + \sum_{n=2}^{\infty} a_n\cos(\lambda_n\tau) + b_n\sin(\lambda_n\tau). \tag{69}$$

The diverging exponential terms in the solution (69) corresponds to the instability of a mass-spring system when the mass is negative so that at an applied (or no) force, there is infinite displacement.

B. Solution of inhomogeneous problem

Assume for the inhomogeneous problem

$$\begin{aligned} \frac{\mathrm{d}v}{\mathrm{d}\tau} &= y + \mathrm{e}^{\mathrm{i}\Omega\tau} \\ \phi(\tau-\kappa_0) + \phi(\tau+\kappa_0) &= y(\tau) \\ \phi(\tau-\kappa_0) - \phi(\tau+\kappa_0) &= v(\tau)\tan\kappa_0, \end{aligned} \tag{71}$$

the trial solution

$$y = A\,\mathrm{e}^{\mathrm{i}\Omega\tau}, \quad v = B\,\mathrm{e}^{\mathrm{i}\Omega\tau}, \quad \phi = C\,\mathrm{e}^{\mathrm{i}\Omega\tau}. \tag{72}$$

Solving (71) with (72), we find

$$A = \frac{\tan\kappa_0}{\Omega\tan(\Omega\kappa_0) - \tan\kappa_0}, \quad B = \frac{-\mathrm{i}\tan(\Omega\kappa_0)}{\Omega\tan(\Omega\kappa_0) - \tan\kappa_0}, \quad C = \frac{\frac{1}{2}\tan\kappa_0\sec(\Omega\kappa_0)}{\Omega\tan(\Omega\kappa_0) - \tan\kappa_0}. \tag{73}$$

From here we can construct solutions for inhomogeneous terms $\cos(\Omega\tau)$ and $\sin(\Omega\tau)$ by taking the real or imaginary part of the solution (72) respectively. At resonance, when $\Omega\tan(\Omega\kappa_0) - \tan\kappa_0 = 0$, we take the trial solution

$$\begin{aligned} y = A\tau\,\mathrm{e}^{\mathrm{i}\Omega\tau}, \quad v = B\tau\,\mathrm{e}^{\mathrm{i}\Omega\tau}, \quad \phi = C\tau\,\mathrm{e}^{\mathrm{i}\Omega\tau} \\ \text{hence} \quad A = \frac{1}{\mathrm{i}\Omega}, \quad B = 1, \quad C = \frac{1}{\mathrm{i}\Omega}\sec(\Omega\kappa_0). \end{aligned} \tag{74}$$

From (74), we see that the solution grows with time and secular terms appear.

C. Order ε^2 equation

Using (33), (34), (38), (39) and (40) with (42), we obtain

$$\begin{aligned} &\cot\kappa_0\left[\tilde\phi_2'(\tilde\tau-\kappa_0) - \tilde\phi_2'(\tilde\tau+\kappa_0)\right] - \left[\tilde\phi_2(\tilde\tau-\kappa_0) + \tilde\phi_2(\tilde\tau+\kappa_0)\right] = \\ &\quad - \sigma\kappa_0\,\mathrm{cosec}\,\kappa_0(A_1\cos\tilde\tau + B_1\sin\tilde\tau) \\ &\quad - \sigma\cos\kappa_0\,(A_1\cos\tilde\tau + B_1\sin\tilde\tau + \sigma A_0\kappa_0\cot\kappa_0\cos\tilde\tau) \\ &\quad + r\cos\kappa_0\,(-A_1\sin\tilde\tau + B_1\cos\tilde\tau - \sigma A_0\kappa_0\cot\kappa_0\sin\tilde\tau) \\ &\quad + \frac{1}{\pi}A_0^2\cos^2\kappa_0\left[r\sum_{n=1}^{\infty}\frac{\cos(2n+1)\tilde\tau}{(n^2-\frac{1}{4})(n+\frac{3}{2})\,[2n+1-\tan\kappa_0\cot(2n+1)\kappa_0]}\right. \\ &\qquad\qquad \left. - 2\sigma\sum_{n=1}^{\infty}\frac{1+\kappa_0\tan\kappa_0+(2n+1)\kappa_0\cot(2n+1)\kappa_0}{(n-\frac{1}{2})(n+\frac{3}{2})\,[2n+1-\tan\kappa_0\cot(2n+1)\kappa_0]}\sin(2n+1)\tilde\tau\right] \\ &\quad + 2A_0\cos^2\kappa_0\left[-A_1\sin\tilde\tau + B_1\cos\tilde\tau - \sigma A_0\kappa_0\cot\kappa_0\sin\tilde\tau\right. \\ &\qquad\qquad \left. + \frac{1}{\pi}A_0^2\cos\kappa_0\sum_{n=1}^{\infty}\frac{\cos(2n+1)\tilde\tau}{(n^2-\frac{1}{4})(n+\frac{3}{2})\,[2n+1-\tan\kappa_0\cot(2n+1)\kappa_0]}\right]|\sin\tilde\tau| \\ &\qquad + \theta_1\sin(\tilde\tau+\theta_0) \end{aligned}$$

References

[1]C. Bréard, A. Sayma, M. Imregun, A.G. Wilson, and B.J. Tester, "A CFD-based non-linear model for the prediction of tone noise in lined ducts," *7th AIAA/CEAS Aeroacoustics Conference*, 2001, AIAA-2001-2176.

[2]A. McAlpine, M.J. Fisher, and B.J. Tester, ""Buzz-saw" Noise: A Comparison of Modal Measurements with an Improved Prediction Method," *Journal of Sound and Vibration*, Vol. 306, No. 3-5, 2007, pp. 419–443.

[3]J.H.M. Disselhorst and L. van Wijngaarden, "Flow in the Exit of Open Pipes during Acoustic Resonance," *Journal of Fluid Mechanics*, Vol. 99, No. 2, 1980, pp. 293–319.

[4]S.W. Rienstra and A. Hirschberg, "An Introduction to Acoustics," Tech. Rep., Technische Universiteit Eindhoven, 2012, revised and updated version of IWDE 92-06, http://www.win.tue.nl/∼sjoerdr/papers/boek.pdf .

[5]T.H. Melling, "The Acoustic Impedance of Perforates at Medium and High Sound Pressure Levels," *Journal of Sound and Vibration*, Vol. 29, No. 1, 1973, pp. 1–65.

[6]R.E. Motsinger and R.E. Kraft, "Design and Performance of Duct Acoustic Treatment", chapter 14 of *Aeroacoustics of Flight Vehicles: Theory and Practice. Volume 2: Noise Control*. Edited by H.H. Hubbard. Acoustical Society of America, Woodbury NY 1995. Originally published as NASA Reference Publication 1258, Vol. 2, 1991.

[7]A.S. Hersh, B.E. Walker, and J.W. Celano, "Helmholtz Resonator Impedance Model, Part 1: Nonlinear Behavior," *AIAA Journal*, Vol. 41, No. 5, 2003, pp. 795–808.

[8]C.K.W. Tam and K.A. Kurbatskii, "Microfluid Dynamics and Acoustics of Resonant Liners," *AIAA Journal*, Vol. 38, No. 8, 2000, pp. 1331–1339.

[9]C.K.W. Tam, K.A. Kurbatskii, K.K. Ahuja, and Jr.R.J. Gaeta, "A Numerical and Experimental Investigation of the Dissipation Mechanisms of Resonant Acoustic Liners," *Journal of Sound and Vibration*, Vol. 245, No. 3, 2001, pp. 545–557.

[10]C.K.W. Tam, H. Ju, M.G. Jones, and T.L. Parrott, "A computational and experimental study of slit resonators," *Journal of Sound and Vibration*, Vol. 284, 2005, pp. 947–984.

[11]J.M. Roche, L. Leylekian, G. Delattre, and F. Vuillot, "Aircraft Fan Noise Absorption: DNS of the Acoustic Dissipation of Resonant Liners," *15th AIAA/CEAS Aeroacoustics Conference*, 2009, AIAA Paper 2009-3146.

[12]C.K.W. Tam, H. Ju, M.G. Jones, W.R. Watson, and T.L. Parrott, "A Computational and Experimental Study of Resonators in Three Dimensions," *15th AIAA/CEAS Aeroacoustics Conference*, 2009, AIAA Paper 2009-3173.

[13]Q. Zhang and D.J. Bodony, "Numerical Simulation of Two-Dimensional Acoustic Liners with High Speed Grazing Flow," *AIAA Journal*, Vol. 49, No. 2, 2011, pp. 365–382.

[14]D.K. Singh and S.W. Rienstra, "Nonlinear asymptotic impedance model for a Helmholtz resonator liner," *Journal of Sound and Vibration*, Vol. 333, No. 15, 2014, pp. 3536–3549.

[15]U. Ingard, "On the Theory and Design of Acoustic Resonators," *Journal of The Acoustical Society of America*, Vol. 25, 1953, pp. 1037–1061.

[16]S.W. Rienstra, "Impedance Models in Time Domain, Including the Extended Helmholtz Resonator Model," *12th AIAA/CEAS Aeroacoustics Conference, Cambridge, MA, USA*, 2006, AIAA Paper 2006-2686.

[17]R.M.M. Mattheij, S.W. Rienstra, and J.H.M. ten Thije Boonkkamp, *Partial Differential Equations: Modeling, Analysis, Computation*, Society for Industrial and Applied Mathematics, 2005.